Eric M. Refour
Mem. ASME
Robotics and Mechatronics Lab,
Department of Mechanical Engineering,
Virginia Tech,
Blacksburg, VA 24060
e-mail: erefour@vt.edu

Bijo Sebastian
Mem. ASME
Robotics and Mechatronics Lab,
Department of Mechanical Engineering,
Virginia Tech,
Blacksburg, VA 24060
e-mail: bijo7@vt.edu

Raghuraj J. Chauhan
Mem. ASME
Robotics and Mechatronics Lab,
Department of Mechanical Engineering,
Virginia Tech,
Blacksburg, VA 24060
e-mail: raghur1@vt.edu

Pinhas Ben-Tzvi
Professor
Mem. ASME
Robotics and Mechatronics Lab,
Department of Mechanical Engineering,
Virginia Tech,
Blacksburg, VA 24060
e-mail: bentzvi@vt.edu

A General Purpose Robotic Hand Exoskeleton With Series Elastic Actuation

This paper describes the design and control of a novel hand exoskeleton. A subcategory of upper extremity exoskeletons, hand exoskeletons have promising applications in healthcare services, industrial workplaces, virtual reality, and military. Although much progress has been made in this field, most of the existing systems are position controlled and face several design challenges, including achieving minimal size and weight, difficulty enforcing natural grasping motions, exerting sufficient grip strength, ensuring the safety of the users hand, and maintaining overall user friendliness. To address these issues, this paper proposes a novel, slim, lightweight linkage mechanism design for a hand exoskeleton with a force control paradigm enabled via a compact series elastic actuator. A detailed design overview of the proposed mechanism is provided, along with kinematic and static analyses. To validate the overall proposed hand exoskeleton system, a fully integrated prototype is developed and tested in a series of experimental trials. [DOI: 10.1115/1.4044543]

Keywords: actuators and transmissions, compliant mechanisms, grasping and fixturing, multi-body dynamics and exoskelotons, wearable robots

1 Introduction

Recently, research into the development of exoskeletons for assistive or rehabilitative purposes has become an area of prominent focus within the robotics community. Their popularity can be attributed to their capacity to advance the fields of healthcare and medicine, virtual reality and interactive gaming, industrial workplace labor, and military pursuits [1]. Like other exoskeleton systems, hand exoskeletons are designed to augment human motion and restore mobility to regions that have lost functionality. Approximately 19.9 million people in the United States suffer from upper body impairments that affect their ability to lift or grasp objects [2]. Of those people, 6.7 million experience difficulties in grasping everyday objects like a cup or a pencil leading to difficulties in performing activities of daily living (ADLs) like eating or using the bathroom. These impairments can be the result of injuries and diseases such as a broken bones, muscle sprain, stroke, spinal cord injury, or cerebral palsy [2]. The variety of hand disabilities can be broadly classified into two categories based on the degree of severity. For individuals who suffer long term and permanent hand impairments, hand exoskeletons are designed to *assist* in grasping motions [3,4]. Individuals who have the potential to recover from their impairments through physical therapy can use hand exoskeletons as *rehabilitation* devices [5–7]. Beyond medical applications, hand exoskeletons are used to create realistic experiences for users through haptic feedback that mimic the sensation of interacting with an object in a virtual reality environment [8,9].[1,2] In an industrial or military settings, hand exoskeletons are used for teleoperation and fatigue reduction by providing enhanced grip strength [10].[3]

To address the wide variety of the above-mentioned applications, there exist two primary mechanical categorizations of hand exoskeletons: rigid link designs and soft designs. The first approach uses rigid links and joints that correspond to those of the human hand [11–16].[4] Most often the linkages are placed on top of the hand as the size of the mechanism exceeds the available space between digits. The use of rigid links also allows for a more direct transmission of power and if designed well, can guarantee that the joint angles enforced onto the user resemble the natural bending profiles of the digits. Furthermore, the rigid structure ensures a measure of repeatability necessary in intelligent grasping control schemes based on discrete kinematic configurations such as that presented in Ref. [17] or accurate force transmission to implement the contact force based controller in Ref. [18]. The price of these advantages is a device that is often bulky, heavy, and/or obstructive to the natural range of motion (RoM) of the hand as well as inducing premature fatigue to the user due to the size and weight of the system.

Many designs have been proposed with soft materials instead of rigid links. The two common implementations use tendon-driven mechanisms [6,19–21] or inflatable membranes that bend to achieve the desired flexion and extension profiles [3,22–25]. The soft design approach allows for a lightweight mechanism that is relatively smaller than most rigid hand exoskeletons. The drawbacks of the tendon-driven gloves include discomfort caused by the cable pre-tension, loss of efficiency caused by friction along the tendon paths, and the shear forces developed in the soft material by the tendon cables while bending. Together these factors hinder

Contributed by Mechanisms and Robotics Committee of ASME for publication in the Journal of Mechanisms and Robotics. Manuscript received February 28, 2019; final manuscript received July 25, 2019; published online September 3, 2019. Assoc. Editor: Med Amine Laribi.

[1] http://www.cyberglovesystems.com/cybergrasp/
[2] https://www.dextarobotics.com/en-us
[3] https://www.festo.com/group/en/cms/10233.htm
[4] See Note 1.

effective force transmission through the tendon system, leading to a loss of repeatability. The soft mechanisms made with inflatable elastic polymers are often unable to provide natural bending profiles for the users digits. In addition, the pneumatic and hydraulic actuators used in these mechanisms have portability issues. They need compressed fluid which leads to a limited operating time when using small fluid tanks; also they have difficulty implementing high-level force and position control.

This work proposes a novel hand exoskeleton that does not suffer the drawbacks of other rigid and soft hand exoskeleton designs. The proposed system, shown in Fig. 1, is a general-purpose hand exoskeleton. Like traditional design approaches, the proposed design consists of linkages that allow for improved alignment and force transmission to the users' joints in a small, lightweight profile comparable to soft hand exoskeletons. In doing so, the proposed design combines the advantages of the traditional and soft glove exoskeleton designs. Few existing designs offer precise force control on each finger, an important prerequisite for implementing intelligent grasp control, whereas the proposed design is capable of both precisely moving the finger joints while fully monitoring their task space. These are the major factors that set apart the proposed design from the existing state-of-the-art exoskeleton glove designs.

This design is an extension of the initial concept proposed previously [26], which presented a two-digit glove with pneumatic actuation. The linkage mechanism is compact enough to be placed between the fingers, thereby heavily reducing the envelope of the system. This paper focuses on optimizing the design parameters of the previous work in order to synthesize an effective assistive device as explained in Sec. 2.2 while extending the design to all the digits with the added capability of ad/abduction on the middle and ring fingers as shown in Figs. 1(*b*) and 1(*c*). This paper also proposes a novel compact series elastic actuator (SEA) design along with a force control framework to allow for individual force control at each finger of the glove thereby improving the grasp performance of the proposed design.

An overview of the linkage mechanism as well as the SEA is presented in Sec. 2 along with the kinematic and static analysis of the proposed force controller. Section 3 presents the prototype integration while Sec. 4 describes experimental analysis. Section 5 concludes the work by summarizing the contributions made along with a discussion of the future work.

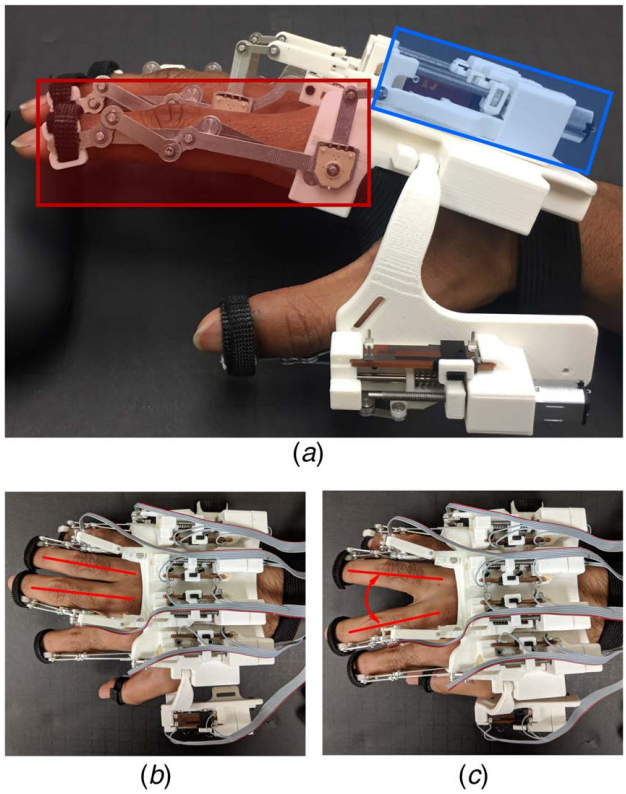

Fig. 1 The completed prototype hand exoskeleton (*a*) where the linkage mechanism is highlighted and the actuator is highlighted. The finger adduction (*b*) and abduction (c) capability of the exoskeleton are also shown and the motion is indicated by the arrows.

2 System Design

The design of the system begins by presenting an analysis of a kinematic model of the human hand and a literature review of the motion and forces exhibited by the fingers. These values are used to determine the desired joint angles for the finger linkage mechanism and the actuator, respectively.

2.1 Human Hand Modeling. To design a mechanism that properly fits the digits and mimics their natural bending profiles during grasping while providing adequate grip strength, the anatomy and functionality of the human hand must be considered. The fingers consist of three phalanges (proximal, middle, and distal) and three main joints (metacarpophalangeal (MCP), proximal interphalangeal (PIP), and distal interphalangeal (DIP)) that are responsible for a large majority of the hand motion. Similarly, the thumb consists of two phalanges (proximal and distal) and three primary joints (trapeziometacarpal (TM), MCP, and interphalangeal (IP)). Additionally, the fingers and thumb are capable of adduction and abduction leading to a total of 21 DOF as per the kinematic model formulated in Ref. [27].

To the authors' knowledge, the most recent and commonly used characterization of human grasping is defined in the GRASP taxonomy, with 33 possible grasps [28]; however, the cylindrical power grasp and the tip-pinch precision grasp are the most common in ADLs [28,29]. Studies from Ref. [30] measured the average digit joint angles of users performing cylindrical power grasps. The analysis in Ref. [31] focused on the joint angle relationships of users performing a tip-pinch grasp. The power grasps were performed on cylindrical pillars of various diameters (2–8 cm), whereas in the tip-pinch experiments, the grasp was held with a grip strength of 100 g while maintaining a pulp distance of 3 cm from the held object. Table 1 presents the resulting data from these studies that serve as the guideline for this work.

To measure the grip strength of healthy individuals performing a cylinder power grasp, researchers in Ref. [32] developed a force-sensing glove that measures the contact pressure on each phalange of the finger. From the 24 volunteers in the experiment, the average phalange forces were 27.6 N (index), 38.5 N (middle), 29.3 N (ring), and 15.3 N (pinky). The sum of the measured phalange forces closely resembles the results found by Mathiowetz et al. [33], which analyzed the cylinder power grip strength of 628

Table 1 Natural joint angles during cylinder power and tip-pinch grasps

	Joint angles (mean, σ)		
	MCP	PIP/IP	DIP
Cylinder power			
Index finger	40 deg, 15 deg	56 deg, 17 deg	37 deg, 12 deg
Middle finger	53 deg, 20 deg	59 deg, 17 deg	35 deg, 15 deg
Ring finger	60 deg, 23 deg	60 deg, 18 deg	30 deg, 18 deg
Pinky finger	–	41 deg, 20 deg	38 deg, 13 deg
Thumb	–	30 deg, 15 deg	–
Tip-pinch			
Index finger	36 deg, 9 deg	35 deg, 16 deg	37 deg, 9 deg
Thumb	12 deg, 8 deg	24 deg, 12 deg	–

healthy volunteers using the Jamar dynamometer and their tip-pinch strength using a B&L pinch gauge. These results form the dictated force requirements for the proposed SEA design.

Based on the above discussion, the design requirements for the glove are summarized below:

(1) The system should be small enough to be worn without drastically affecting the users perceived hand space or restricting the natural RoMs for their digits and wrist. The height of the system should not exceed 35 mm from the dorsum of the hand. This height was chosen based on the dimensions of a state-of-the-art linkage based hand exoskeleton design [14], which has a height of 35 mm.
(2) The hand exoskeleton should be lightweight so as to not induce premature fatigue while assisting with ADLs. The proposed system should weigh no more than 430 g which is the weight of one of the lightest state-of-the-art linkage based gloves, the SAFER Glove [11].
(3) The mechanism should be capable of producing natural bending profiles for the fingers and thumb. The natural joint angles from Table 1 are used to design the desired profiles.
(4) The proposed hand exoskeleton should perform commonly used grasps with a force that resembles the natural grip strengths of a healthy human hand. The desired force output from each digit should be within the range of 15–30 N which corresponds to the force output from several state-of-the-art gloves [11,14,19,24,34–36].
(5) The RoM provided by the mechanism must match the safe RoM for the corresponding digit in order to ensure safety of the user while operating the device.

The proposed design will be able to overcome the common issues of hand exoskeletons that were discussed in Sec. 1. The proposed design addresses all of the above requirements under the following assumptions:

(1) The MCP, DIP, and PIP joints are coupled and the relationship between the joint angles remains fixed for the range of motion produced by the exoskeleton. Even though this assumption does not hold while taking into account all of the 33 characterized grasps, it holds well enough for the considered cylinder power and pip-pinch grasps.
(2) The revolute joints of the mechanism are fairly well aligned with the corresponding joints on the human hand. The tip of the mechanism is securely fixed onto the fingertips of the patient without any slip. In order to satisfy these assumptions, the proof of concept prototype described in this paper was built according to the hand dimensions of one of the authors, on whom the device was tested. As such, the proposed design needs to be custom made for each user like most commercially available active prosthetic devices.

Even though the above assumptions limit the variety of grasps that can be accurately reproduced by the glove, providing additional degrees of freedom and corresponding actuators to allow for the variation in the kinematic relationship between the finger joints will result in a bulkier system, thereby reducing its overall usability. This results in a tradeoff between the effectiveness of the glove in reproducing a wide range of grasps and the overall ergonomics of the device. The design is proposed on the hypothesis that a reduced dimensionality system, while being effective only for several grasps, will be lightweight and compact and increase its overall effectiveness as an assistive exoskeleton system, which in turn adds to the novelty of the work.

2.2 Linkage Mechanism Synthesis and Kinematics. The linkage-based exoskeleton design described here was first used in developing a two-digit pneumatic prototype [26]. The old design was optimized and refined to produce the slim, compact, and form fitting full hand exoskeleton presented here. Figures 2 and 3 show the linkage design which consists of planar links and revolute joints that correspond to the joints and phalanges of the digits. The thumb mechanism consists of one four bar linkage, whereas the finger mechanisms consist of two four bar linkages in series. The five links and seven joints have been separately shown as two four-bar mechanisms in Fig. 2. For a detailed description on the working of the proposed mechanism, interested readers are referred to Ref. [26]. The kinematic formulation of the proposed mechanism is described below. This formulation will be used for the static analysis and for the optimization of design parameters.

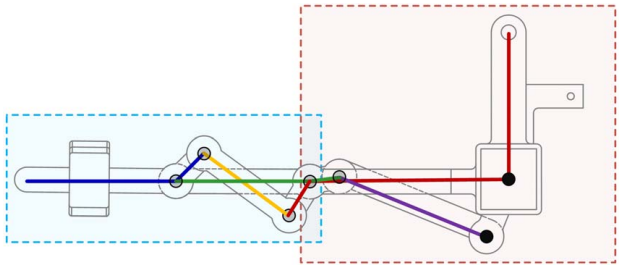

Fig. 2 The layout of the dual four-bar mechanism for a single finger. The boxes denote the first and second four-bars. The circles are the revolute joints with the filled circle denoting the revolute joints attached to the ground frame. The individual linkages are shown by the thicker lines starting from the base of the finger to the tip.

The design parameters are shown in Fig. 3 where l_i is defined as the length of the phalange of the intended wearer. Subscripts 1, 2, and 3 correspond to the middle, proximal, and distal phalange, respectively. From here on, these linkages will be referred to as

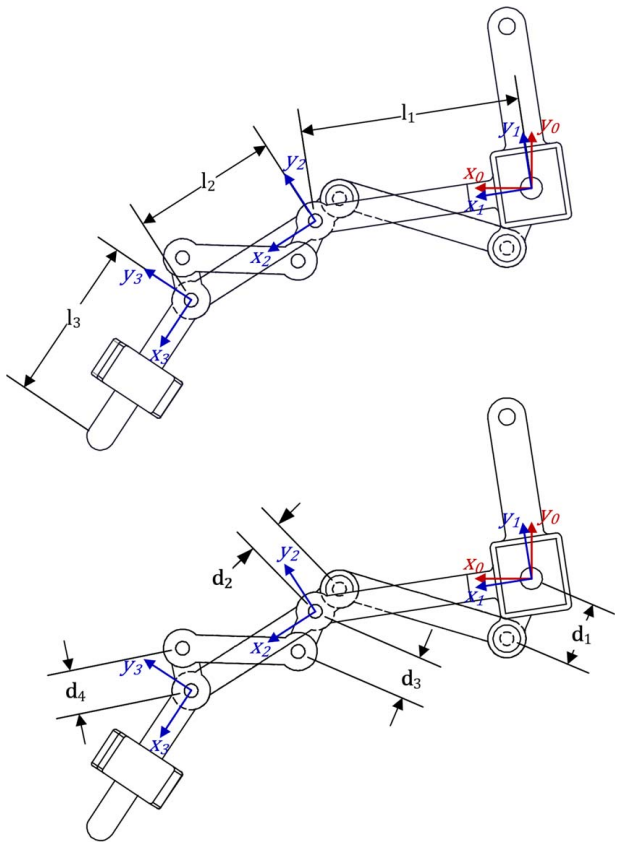

Fig. 3 The bent configuration of the finger with the design parameters l_i, d_j, where $i \in \{1, 2, 3\}$, $j \in \{1, 2, 3, 4\}$. The reference frames attached to each phalange associated linkage are denoted as x_i, y_i, where $i \in \{1, 2, 3\}$ and the frame x_0, y_0 is the ground frame attached the glove base

their length variables, l_i. The local reference frame for each linkage, F_i, is defined by x_i, y_i. The parameters $\mathbf{d}_j$ are defined as the location vector of the relative distance constraints between revolute joints on each linkage pair as defined below and shown in Fig. 2.

$\mathbf{d}_1$ The relative distance between l_2 and the ground frame defined in f_0. $\mathbf{d}_1 \longleftarrow \mathbf{d}_1^0$.
$\mathbf{d}_2$ The relative distance between l_2 and the ground frame defined in f_2. $\mathbf{d}_2 \longleftarrow \mathbf{d}_2^2$.
$\mathbf{d}_3$ The relative distance between l_3 and l_1 defined in f_1. $\mathbf{d}_3 \longleftarrow \mathbf{d}_3^1$.
$\mathbf{d}_4$ The relative distance between l_3 and l_1 defined in f_3. $\mathbf{d}_4 \longleftarrow \mathbf{d}_4^3$.

As such, the pairs $\mathbf{d}_1^0$, $\mathbf{d}_2^2$ and $\mathbf{d}_3^1$, $\mathbf{d}_4^3$ correspond to the distance constraint between the linkage pairs, given by

$$\begin{aligned} c_1 &= \left\| \begin{bmatrix} l_1 \\ 0 \end{bmatrix} + \begin{bmatrix} -1 & 0 \\ 0 & 1 \end{bmatrix} (\mathbf{d}_1^0 + \mathbf{d}_2^2) \right\|_2 \\ c_2 &= \left\| \begin{bmatrix} l_2 \\ 0 \end{bmatrix} + \begin{bmatrix} -1 & 0 \\ 0 & 1 \end{bmatrix} (\mathbf{d}_4^3 + \mathbf{d}_3^1) \right\|_2 \end{aligned} \tag{1}$$

In this formulation, the joint angles associated with the MCP, PIP, and DIP joints are θ_i where $i \in 1, 2, 3$ and θ_i is the rotation from f_{i-1} to f_i.

For any given set of $\mathbf{d}_j$ parameters, the entire system can be formulated as a constraint based kinematic model. The three DOFs associated with each linkage member l_i are contained in $\mathbf{q}$ defined by

$$\begin{aligned} \mathbf{q} &= \begin{bmatrix} x_1, & y_1, & \theta_1, & x_2, & y_2, & \theta_2, & x_3, & y_3, & \theta_3 \end{bmatrix}^T \\ &= \begin{bmatrix} \mathbf{r}_1, & \theta_1, & \mathbf{r}_2, & \theta_2, & \mathbf{r}_3, & \theta_3 \end{bmatrix}^T \end{aligned} \tag{2}$$

A corresponding kinematic constraint vector, $\mathbf{\Phi}^k$, for the linkage system is defined as

$$\begin{aligned} \mathbf{\Phi}^k &= \begin{bmatrix} (\theta_1 - \alpha(t)), & \Phi_{0,1}^{r\,T}, & \Phi_{1,2}^{r\,T}, & \Phi_{2,3}^{r\,T}, & \Phi_{0,2}^{d\,T}, & \Phi_{1,3}^{d\,T} \end{bmatrix}^T \\ &= \mathbf{0}_{9\times 1} \end{aligned} \tag{3}$$

where $\alpha(t)$ is the driving constraint, $\Phi_{i,j}^r \in \mathbb{R}^{2\times 1}$ are the revolute joints, and $\Phi_{i,j}^d \in \mathbb{R}^{1\times 1}$ are the relative distance constraints between bodies i and j as given by

$$\Phi_{i,j}^r = \begin{bmatrix} \mathbf{r}_j'^R - \mathbf{r}_i'^R \end{bmatrix} \tag{4}$$

$$\Phi_{i,j}^d = \begin{bmatrix} (\mathbf{r}_j'^D - \mathbf{r}_i'^D)^T (\mathbf{r}_j'^D - \mathbf{r}_i'^D) - C^2 \end{bmatrix} \tag{5}$$

where $r_{i/j}'^{R/D}$ is the location of the revolute or relative distance constraint point joint on body i/j in the local frame. Therefore, the locations of the points $r_{i,j}'^{R/D}$ are the locations of the revolute joints in Fig. 2. The values for C are determined using Eq. (1).

2.3 Optimization of Design Parameters. The angle of the body, l_1, for the purpose of this optimization will be defined as a function of time, $\theta_1(t)$. The revolute and relative distance constraints are defined as given below. As stated previously, the goal of the optimization process was to determine values of $\mathbf{d}_j$ given l_i for each finger to best match the finger joint angles in Table 1 while keeping the height of the mechanism as low as possible to limit how far it extends above and below each finger.

The overall optimization procedure can be summarized as follows, for a given set of design parameters $\mathbf{d}_j$, the constrained kinematic model can be solved for $\mathbf{q}$ with $\alpha(t)$ going from 0 to the maximum MCP joint angle using the Newton–Raphson method. The joint angles, produced by the mechanism namely θ_i, are then compared with the desired natural joint angles as given in Table 1. In addition, the chosen $\mathbf{d}_j$ must ensure that the size of the mechanism falls within the design requirements. This is expressed in the form of linear inequality constraint along with upper and lower bounds on the possible values of the design variables.

The following objective function was used for optimizing the design parameters for each finger:

$$F_{\min}(\theta) = \sum_{i=1}^{3} w_i \tilde{\theta}_i \tag{6}$$

subject to

$$\mathbf{AD} \leq \mathbf{b} \tag{7}$$

$$\mathbf{l}_b \leq \mathbf{D} \leq \mathbf{u}_b \tag{8}$$

where $\mathbf{D} \in \mathbb{R}^{8x1}$ is the vector of the optimization variables, $\tilde{\theta}_i$ is the error between the desired and optimized finger joint angles, w_i is a tuneable weight variable, $\mathbf{A}$ and $\mathbf{b}$ form the linear inequality constraint, and $\mathbf{l}_b$ and $\mathbf{u}_b$ are the lower and upper bounds of the decision variables.

The optimization was performed using the interior-point algorithm in MATLAB. The results of the optimization are presented in Table 2.

2.4 Linkage Statics. The following section analyses the behavior of the linkage mechanism when the fingertips of the user contact the environment. For the purpose of this analysis, the mechanism can be considered as a three body kinematic chain each with three DOFs. Based on this assumption, the Jacobian J_3^0 can be used to determine the force at the finger tip as given by

$$\boldsymbol{\tau} = -J_3^{0\mathrm{T}} \mathbf{F}_3^0 \tag{9}$$

where $\boldsymbol{\tau}$ is the vector of joint torques at each of the three joint locations, $\mathbf{F}_3^0$ is the vector of forces at the fingertip, and J_3^{0T} is

$$J_3^{0T} = \begin{bmatrix} -l_1 \sin(\theta_1) & l_1 \cos(\theta_1) & 1 \\ -l_2 \sin(\theta_2) & l_2 \cos(\theta_2) & 1 \\ -l_3 \sin(\theta_3) & l_3 \cos(\theta_3) & 1 \end{bmatrix} \tag{10}$$

For the two major grasps that form the focus of this paper, cylinder and tip pinch, a large majority of the contact tip force of each finger is aligned with the global x_0 axis. This allows further simplification as $\mathbf{F}_3^0 = [F_c, 0, 0]^T$ Therefore, only the first row of Eq. (9) needs be considered. Solving for τ_1 leads to the following expression:

$$\tau_1 = -l_1 \sin(\theta_1) F_c \tag{11}$$

The above simplified expression will be used in determining the SEA forces as described in Sec. 2.5.

2.5 Actuator Design. The proposed design of the SEA is shown in Fig. 4. This design is greatly inspired by existing state-of-the-art SEA design [37]. The proposed design consists of four primary components: a motor, a leadscrew, compression springs, and the actuator output point. A Pololu micrometal gearmotor was attached to the leadscrew to achieve the desired linear motion. The output is coupled to the leadscrew nut by the

Table 2 The optimized mechanism finger joint angles

	Joint angles		
	MCP	PIP/IP	DIP
Index finger	39.06	28.88	25.28
Middle finger	44.95	38.85	29.91
Ring finger	45.03	39.34	33.41
Pinky finger	38.70	34.84	34.57
Thumb	20.12	24.01	–

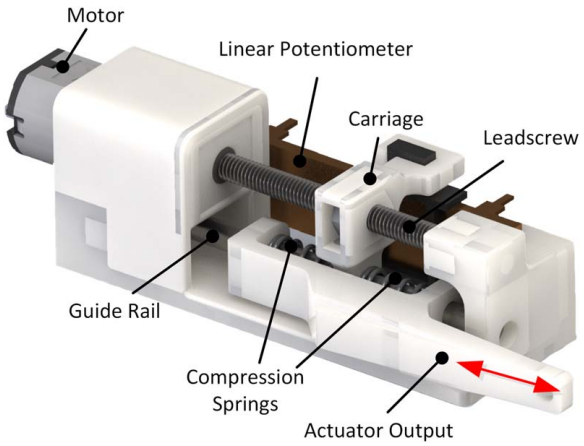

Fig. 4 The design of the SEA used for the exoskeleton glove with the direction of actuation indicated by the arrow

compression springs. A single spring is used on either side of the leadscrew nut so that elasticity is achieved for both flexing and extending the finger mechanism. A linear potentiometer is used to measure the position of the actuator prior to the elastic element.

The linear force of the leadscrew can be calculated using the standard equation for the raising of a leadscrew (force opposing the direction of motion):

$$F_{lead} = \frac{2\tau_m}{d_m \tan(\phi - \lambda)} \tag{12}$$

where F_{lead} is the linear force of the leadscrew, τ_m is the motor torque, d_m is the mean diameter of the leadscrew, ϕ is the angle of friction based on the coefficients of friction of the leadscrew and nut, and λ is the lead angle based on the pitch of the leadscrew.

To determine the compression of the springs, the layout of the actuator and linkage mechanism must be considered first. The layout is given in Fig. 5, where the configurations with and without spring deflection is shown. The carriage in Fig. 5 corresponds to the carriage shown in Fig. 4. Another linkage is used to connect the finger mechanism to the actuator and is defined by the length r_2. The lengths r_1, r_2, and h are part of the design parameters and are therefore fixed. The variable x_{SEA} is the position of the actuator measured by the linear potentiometer, as summed with the uncompressed spring length in the f_0 frame. The angle θ_1 is measured using a rotary potentiometer. As such, the spring deflection,

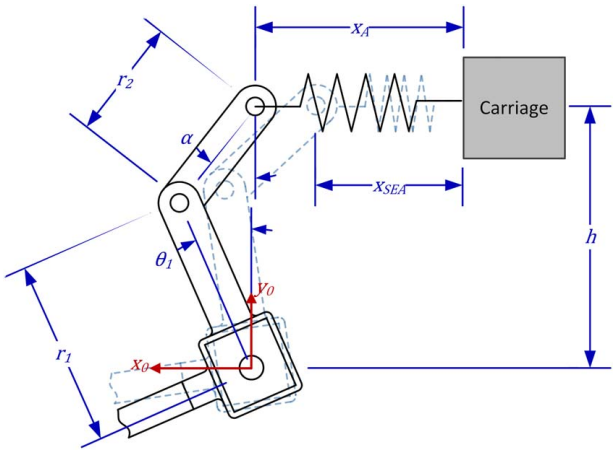

Fig. 5 The layout of the SEA and the finger mechanism showing a user deflected configuration (black) and the uncompressed configuration (grey)

Δx_s, and thereby the SEA force can be calculated as

$$\alpha = \cos^{-}1\left[\frac{h - r_1 \cos(\theta_1)}{r_2}\right] \tag{13}$$

$$x_A = r_1 \sin(\theta_1) - r_2 \sin(\alpha) \tag{14}$$

$$F_{SEA} = k(x_A - x_{SEA}) \tag{15}$$

where k is the spring constant of the elastic members in the actuator and F_{SEA} is the force due to the actuator in the f_0 frame. The conversion from this force to the effective contact force at the finger tip is found by substituting Eq. (15) into Eq. (11):

$$F_{SEA} = \frac{-l_1 F_C \tan(\theta_1)}{h} \tag{16}$$

The measurements for x_{SEA} and θ_1 are used to convert the desired contact force into the requisite SEA force. Now, given a desired grasping force at each fingertip, a target actuator spring displacement can be calculated using Eq. (16). A proportional integral derivative (PID) controller for the motor in the SEA was implemented as shown in Fig. 6. An estimate of the force applied by the SEA is fedback to the closed loop PID controller which then drives the motor until the mechanism exerts the desired grasp force. Naturally, the implementation of the controller as shown in Fig. 6 required saturation limits to be placed on the range of x_{SEA} so as to not damage the system.

3 Prototype Integration

To develop the full prototype, the mechanism design was refined for manufacturing and the required electronics were incorporated.

3.1 Mechanical Design. The conceptual design of the proposed mechanism from Sec. 2 was further developed using SolidWorks. As shown in Fig. 1, the design incorporates the necessary sensors and fixture points for the mechanism links and the users hand. The links were manufactured using 6061 aluminum and the fingertip attachment pieces with Velcro straps were 3D printed with acrylonitrile butadiene styrene (ABS) plastic. To fix all of the digit mechanisms to a supporting frame, a dorsal hand base was designed. The thumb mechanism is fixed to its own base that is attached to the main hand base via a motor shaft that actuates the corresponding DOF for abduction/adduction. To allow for the passive abduction and adduction, a hinge joint was designed for the middle and ring finger mechanisms as shown in Figs. 1(*b*) and 1(*c*). The addition of this passive degree of freedom makes it easier for users to adjust finger positions while grasping different objects. The outer fingers (index and pinky finger) were directly attached to the glove base. The drive-train, output carriage, and overall SEA housing units for the motors were 3D printed in ABS plastic. Compression springs rated at 9.27 N/mm with a free length of 9.65 mm and a maximum deflection of 4.32 mm were used in the SEA. Approximately 49.41 N is required to fully compress these springs. From Eq. (16), this leads to a maximum theoretical contact force of 38.03 N on each of the fingers, which is above the desired maximum of 30 N as mentioned in Sec. 2.

To achieve a grip strength that closely resembles that of a normal hand (as mentioned in Sec. 2.1), Pololu micro gear motors of appropriate torque rating were chosen. These enable flexion and extension motions with a maximum theoretical force exceeding 32.91 N using Eq. (12) and the values presented in Table 3. The gearbox efficiency was experimentally found to be approximately 52%.

3.2 Electronic Design. To measure the value of θ_1 for each finger, Bourns 3382 rotary position sensors were used and placed at the MCP joints. A digital protractor was used to manually

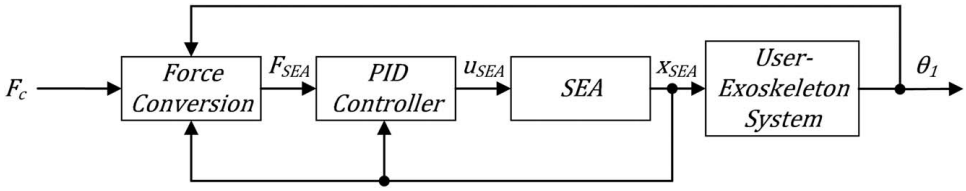

Fig. 6 The control diagram for the SEA based on a desired contact force

Table 3 The leadscrew and motor parameters

Parameter	Value
τ_m	0.156 Nm
d_m	2.675 mm
ϕ	0.611 rad
λ	0.059 rad

calibrate the encoder values into corresponding angular measurements. Since the MCP joints of the mechanisms were designed to correspond to the MCP joints of the fingers and thumb, the use of rotary encoders provided close measurements for the user MCP digit joints during grasping motions. The remaining PIP and DIP joints for the finger and IP joint for the thumb were calculated using the kinematic model of the mechanisms as presented in Sec. 2. For the lead screw position measurement inside the SEA, linear slide potentiometers from All Electronics Corp. were selected. These thin profile potentiometers are rated at 20 kΩ. They provide a travel distance of 0.85 in (21.60 mm), which gives an overall stroke length of 19 mm from the SEA modules.

A Teensy 3.6 was used as the microcontroller unit for implementing the force control algorithms. Featuring a 32-bit, 180 MHz clock frequency ARM Cortex-M4 microprocessor, the Teensy 3.6 provides sufficient speed, memory size, and computational performance for the proposed application and for future implementations of intelligent grasp routines. In order to integrate the sensors and actuators together with the microcontroller unit, a custom printed circuit board (PCB) was designed and developed for the system (as shown in Fig. 7). To provide an alternative means of commanding the exoskeleton to perform a grasp, tactile pushbuttons were added to the PCB.

4 Experimental Validation

To validate the various functions of the proposed hand exoskeleton, several experiments were performed as summarized below.

4.1 Joint Angle Relationship and Workspace Experiment. To ensure that the proposed hand exoskeleton is capable of producing natural bending profiles onto the joints of the users digits, a study was performed. The focus of the experiment was to measure and compare the joint angles enforced by the digit mechanisms with the desired normal joint angles from Table 1. The experiment was performed by mounting the digit mechanism onto a wooden mannequin hand and actuating the digits to perform a full flexion motion. During the flexion and extension motion, the joints of the mannequin digits were tracked using a GoPro HERO4 Session 10 MP camera. To measure the joint angle displacements produced in the mannequin hand by the exoskeleton, visual markers were placed on each of the phalanges. A MATLAB script was then used to track the motion of the markers from the image frames and thereby estimate the individual joint angles. The experimental setup used for visual tracking of the joints is the same as in Ref. [26]. Interested readers are referred to Ref. [26] for additional details regarding the setup.

The experiments involved using the index finger, middle finger, and thumb as the primary digits to test, since the other two finger mechanisms were built similarly. The experimental results of these digits are shown in Fig. 8. To validate the performance of the glove, the results are plotted alongside the desired joint angles as given in Table 2.

The experiment produced strong results in terms of repeatability as shown by the forward and backward motions of the mechanisms. However, only the thumb was able to meet its optimized value. The failure for the index and middle fingers stems from the mannequin hand deviating in size from the hand of the user for which the glove was designed. This caused the joints to not appropriately align, causing the mechanism to violate the kinematic constraints.

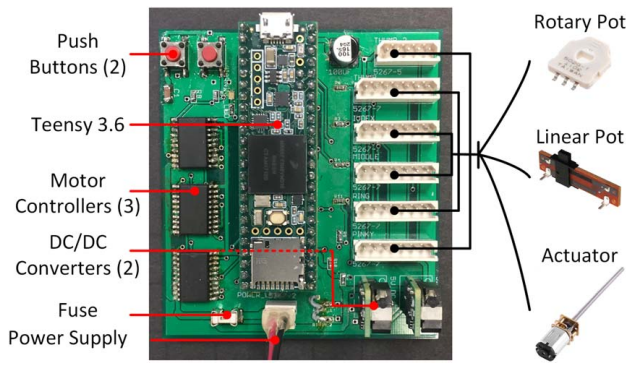

Fig. 7 The PCB along with the key components interfaced with the proposed hand exoskeleton

4.2 Force Control with Series Elastic Actuator Module Experiment. In order to test the performance of the proposed force controller with the SEA modules, an experiment was performed. The SEA unit was commanded to attain three different force values and a TM0-2 load cell by Transducer Techniques was used to measure the true output. For the duration of the experiment, the SEA unit and load cell sensor were fixed to a mechanical breadboard table, as shown in Fig. 9. The load cell was positioned along the path of the output carriage to measure the force that would be applied onto the mechanism lever.

The experiment was performed to test three different desired forces: 10 N, 15 N, and 23 N. The results from each case are plotted in Fig. 10. The best case was the 10 N trial, in which the system reached a maximum of 9.04 N, whereas the worst case was the 15 N trial that outputted 12.7 N. For the 23 N case, the controller was able to achieve an output of 20.9 N. Overall, the results proved that with the proposed force controller and SEA modules, the system is capable of achieving a desired force with an average accuracy of 90%. The force control is formulated under the assumption that the spring stiffness K remains constant for the range of operation. Based on the results shown in Fig. 10, this assumption is not valid especially in case of large forces. The primary source for this nonlinearity, as well as the failure of the system to achieve the desired force, is that 3D printed members of the actuator begin to deflect under load. In that sense, there are multiple, unintended elastic members in the actuator. In the future, the construction of the glove and the SEA module will be modified to improve the overall structural strength and thereby

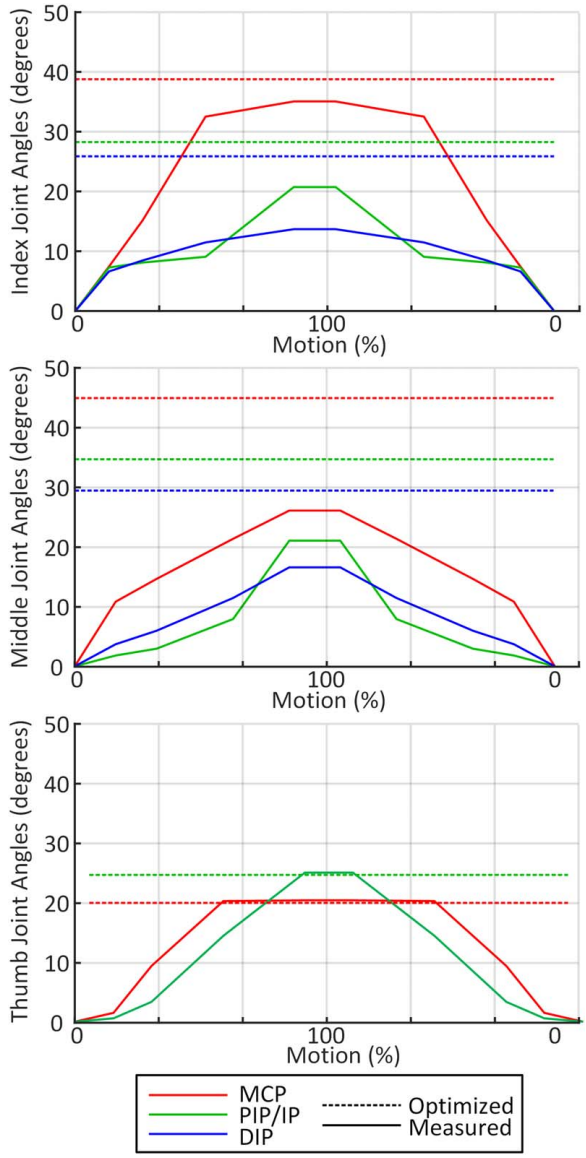

Fig. 8 The joint angles for the index finger, middle finger, and thumb as a percent of the range of motion. The optimized joint angles (small dashes) and measured joint angles (solid) are all shown.

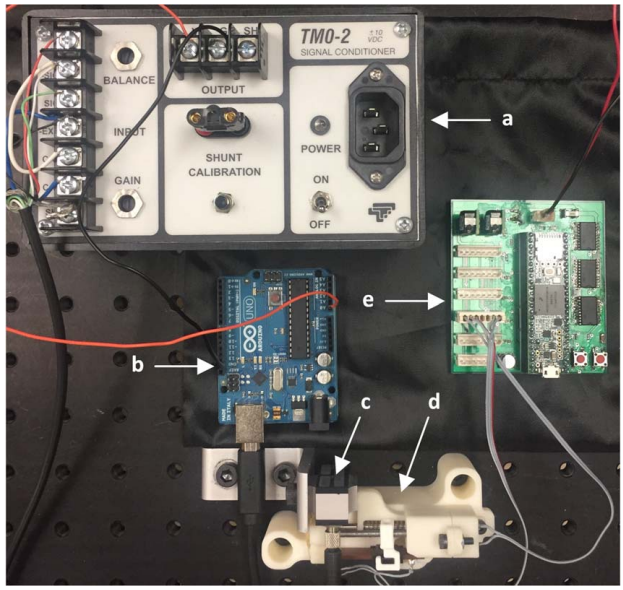

Fig. 9 The experimental setup for the SEA force experiment showing: (a) signal conditioner, (b) microcontroller for reading force measurements, (c) load cell, (d) SEA, and (e) motor controller PCB

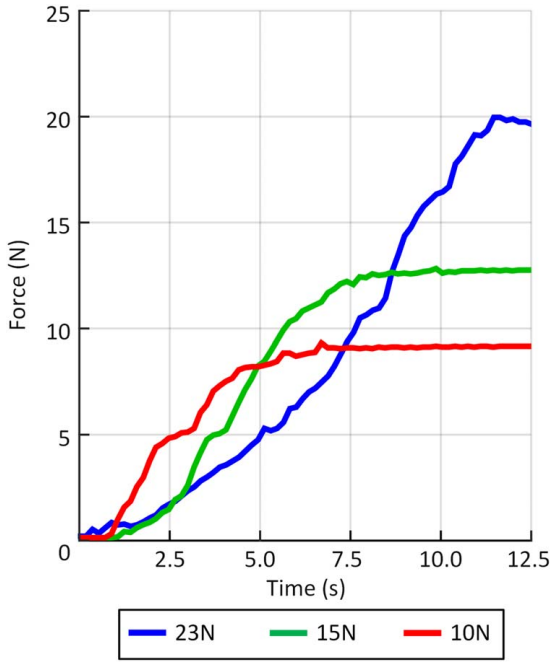

Fig. 10 The results of the SEA force experiment with three target forces

provide deflection only on the intended members. For the purpose of this paper, the force control experiment was done using only the SEA module, and future work will involve force control experiments using the glove for a wide range of grasps.

4.3 Assistive Grasping. To demonstrate the prototypes ability to grasp various objects, benchmarking tests were performed and are presented in Fig. 11 using ordinary objects. For the tests, the user was instructed to wear the prototype while it actively grasped various objects by means of the proposed force controller running for each individual finger mechanism. A review by the institutional review board (IRB) and its approval were not required for these tests, since the Virginia Tech IRB determined that the proposed tests can be classified as research not involving human subjects as defined by the U.S. Department of Health and Human Services (DHHS) and U.S. Food and Drug Administration (FDA). The decision to use a human hand was made since the ideal choice of using a wooden mannequin hand was not feasible due to the aforementioned lack of joint alignment and range of motion. To prevent a healthy hand from impacting the results of the experiment, the user was instructed to relax their hand and let it act passively, only moving when enforced by the hand exoskeleton. Additional cases were performed in which the glove grasped objects alone, without the user hand inserted as shown in Figs. 11(*a*) and 11(*e*).

5 Conclusion and Future Work

This paper presented the design overview, optimization, prototype integration, and experimental validations of a proposed novel hand exoskeleton. The proposed design was developed with specific goals in mind, which were outlined in Sec. 2. Based on these goals and requirements, the novelty and contribution of this proposed design can be summarized into several key features.

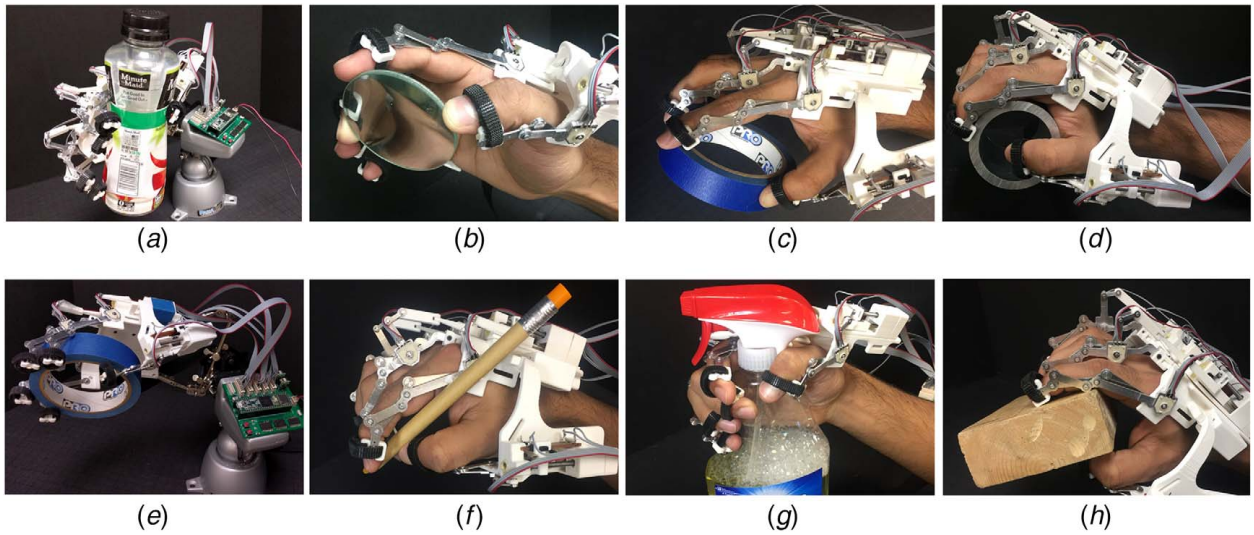

Fig. 11 Grasping test with various everyday objects: (*a*) beverage bottle (glove only), (*b*) magnifying lens, (*c*) tape, (*d*) cylinder-shaped metal, (*e*) tape (glove only), (*f*) pencil, (*g*) cleaning spray, and (*h*) wooden block

- *Size:* The proposed hand exoskeleton was designed to consist of linkage mechanisms small enough to be placed alongside the fingers and thumb. Each digit mechanism is approximately 4.5 mm in width (6.5 mm including joint pins) and is less than 18 mm in height, excluding the lever. The height of the prototype is 20 mm when measured from the hand base and 24.25 mm from the dorsal side of the user hand. Along with the compact SEA modules to provide force control, the proposed design offers a slim compacted hand exoskeleton through all of its small profile features.
- *Wearability:* The design ensures practicality by offering a small profile, lightweight system. The prototype glove weighs only 245 g (excluding a battery source), which is less than half of the targeted weight goal. This allows the system to be portable and comfortable during prolonged usage. In addition, the SEA springs offer compliance during grasping and the ability to implement force controlled grasping.
- *Naturalistic motion:* As shown by the experiment in Sec. 4, the hand exoskeleton can enforce natural joint angles during grasping motions. This ensures that the glove is capable of performing commonly used grasps, allowing it to serve both as an assistive glove and a rehabilitation device.
- *Grip strength:* Using the proposed force controller and compact SEA modules, the hand exoskeleton can produce more than 20 N per digit, to achieve the desired target range.

To achieve the above goals, a mechanism was synthesized based on the author's previous work [26] in which two serially connected four-bar mechanisms are used to couple the motion of the finger joints. An optimization routine was performed based on the kinematics of the linkage in order to best meet the desired finger joint angles while minimizing the size of the mechanism. An SEA was also designed and presented to meet the force requirements of the fingers based on experimental data from the literature. Experimental validation of both the joint angles and the forces was performed.

The focus of this paper was to demonstrate the feasibility of the proposed design, which works under the assumption of having good alignment between the revolute joints of the mechanism and the joint on the human hand. Moreover, the kinematic relationships between the MCP, PIP, and DIP joints are assumed to be fixed in order to produce a light weight portable design. Future work will involve detailed clinical trials under the supervision of a medical practitioner to validate the use of the device as a medical tool. This will provide insights toward determining if the proposed design approach toward improving the overall usability of the glove as compared to accurately reproducing a wide range of grasps is more beneficial to the patient population. In addition, future work will involve analysis of the joint angles and the forces produced by the glove in the case where the mechanism joints are not perfectly aligned with the human hand as explored in Refs. [38,39]. Design modifications will be explored in order to provide adjustable link lengths so that the glove can be used by individuals with differently sized hands rather than custom manufacturing the glove. Additionally, due to the misalignment of the test mannequin and the glove, the angular reproduction by the current prototype was not highly accurate. The results will be improved through more robust manufacturing with stronger materials especially for the actuator to ensure the transmission of force through the proper members. Given the capabilities of this device, intelligent controllers [17,18] allowing for autonomous and adaptive grasping will also be tested and validated as part of future work.

Acknowledgment

Research reported in this publication was supported in part by the Eunice Kennedy Shriver National Institute of Child Health and Human Development of the National Institutes of Health under Award Number R21HD095027. The content is solely the responsibility of the authors and does not necessarily represent the official views of the National Institutes of Health.

References

[1] Bogue, R., 2009, "Exoskeletons and Robotic Prosthetics: A Review of Recent Developments," Industrial Robot, **36**(5), pp. 421–427.
[2] Brault, M. W., 2010, Americans with Disabilities: 2010. U.S. Census 2010 Report. https://www2.census.gov/library/publications/2012/demo/p70-131.pdf
[3] Yap, H. K., Lim, J. H., Nasrallah, F., Goh, J. C., and Yeow, R. C., 2015, "A Soft Exoskeleton for Hand Assistive and Rehabilitation Application Using Pneumatic Actuators With Variable Stiffness," Proceedings — IEEE International Conference on Robotics and Automation, Seattle, WA, May 26–30, pp. 4967–4972.
[4] Ho, N. S. , Tong, K. Y., Hu, X. L., Fung, K. L., Wei, X. J., Rong, W., and Susanto, E. A., 2011, "An EMG-Driven Exoskeleton Hand Robotic Training Device on Chronic Stroke Subjects: Task Training System for Stroke Rehabilitation," Proceedings of IEEE International Conference on Rehabilitation Robotics, Zurich, Switzerland, June 29–July 1.
[5] Maciejasz, P., Eschweiler, J., Gerlach-Hahn, K., Jansen-Troy, A., and Leonhardt, S., 2014, "A Survey on Robotic Devices for Upper Limb Rehabilitation," J. Neuroeng. Rehabil., **11**(1), p. 3.
[6] Lee, S. W., Landers, K. A., and Park, H. S., 2014, "Development of a Biomimetic Hand Exotendon Device (BiomHED) for Restoration of Functional Hand Movement Post-Stroke," IEEE T. Neur. Syst. Rehabil. Eng., **22**(4), pp. 886–898.

[7] Ito, S., Kawasaki, H., Ishigure, Y., Natsume, M., Mouri, T., and Nishimoto, Y., 2011, "A Design of Fine Motion Assist Equipment for Disabled Hand in Robotic Rehabilitation System," J. Franklin Inst., **348**(1), pp. 79–89.
[8] Ma, Z., Ben-Tzvi, P., and Danoff, J., 2016, "Hand Rehabilitation Learning System With An Exoskeleton Robotic Glove," IEEE T. Neur. Syst. Rehabil. Eng., **24**(12), pp. 1323–1332.
[9] Popescu, V. G., Burdea, G. C., Bouzit, M., and Hentz, V. R., 2000, "A Virtual-Reality-Based Telerehabilitation System with Force Feedback," IEEE T. Inf. Technol. B., **4**(1), pp. 45–51.
[10] Shimoga, K., and Khosla, P., 1994, "Touch and Force Reflection for Telepresence Surgery," Proceedings of 16th Annual International Conference of the IEEE Engineering in Medicine and Biology Society, Baltimore, MD, Nov. 3–6, pp. 1049–1050.
[11] Ben-Tzvi, P., Danoff, J., and Ma, Z., 2016, "The Design Evolution of a Sensing and Force-Feedback Exoskeleton Robotic Glove for Hand Rehabilitation Application," ASME J. Mech. Rob., **8**(5), p. 051019.
[12] Heo, P., and Kim, J., 2014, "Power-Assistive Finger Exoskeleton With a Palmar Opening At the Fingerpad," IEEE T. Biomed. Eng., **61**(11), pp. 2688–2697.
[13] Agarwal, P., Fox, J., Yun, Y., O'Malley, M. K., and Deshpande, A. D., 2015, "An Index Finger Exoskeleton With Series Elastic Actuation for Rehabilitation: Design, Control and Performance Characterization," Int. J. Robot. Res., **34**(14), pp. 1747–1772.
[14] Jo, I., and Bae, J., 2017, "Design and Control of a Wearable and Force-controllable Hand Exoskeleton System," Mechatronics, **41**(2), pp. 90–101.
[15] Chiri, A., Giovacchini, F., Vitiello, N., Cattin, E., Roccella, S., Vecchi, F., and Carrozza, M. C., 2009, "HANDEXOS: Towards an Exoskeleton Device for the Rehabilitation of the Hand," Proceedings of IEEE/RSJ International Conference on Intelligent Robots and Systems, St. Louis, MO, Oct. 10–15, pp. 1106–1111.
[16] Iqbal, J., Ahmad, O., and Malik, A., 2011, "HEXOSYS II — Towards Realization of Light Mass Robotics for the Hand," Proceedings of the 14th IEEE International Multitopic Conference, Karachi, Pakistan, Dec. 22–24, pp. 115–119.
[17] Chauhan, R. J., and Ben-Tzvi, P., 2018, "Latent Variable Grasp Prediction for Exoskeletal Glove Control," Proceedings of ASME Dynamic Systems and Control, Atlanta, GA, Sep. 30–Oct. 3.
[18] Lee, B. J., Williams, A., and Ben-Tzvi, P., 2018, "Intelligent Object Grasping With Sensor Fusion for Rehabilitation and Assistive Applications," IEEE T. Neur. Syst. Rehabil. Eng., **26**(8), pp. 1556–1565.
[19] In, H., Kang, B. B., Sin, M. K., and Cho, K. J., 2015, "Exo-Glove: A Wearable Robot for the Hand With a Soft Tendon Routing System," IEEE Robot. Autom. Mag., **22**(1), pp. 97–105.
[20] Nycz, C. J., Delph, M. A., and Fischer, G. S., 2015, "Modeling and Design of a Tendon Actuated Soft Robotic Exoskeleton for Hemiparetic Upper Limb Rehabilitation," Proceedings of the Annual International Conference of the IEEE Engineering in Medicine and Biology Society, Milan, Italy, Aug. 25–29, pp. 3889–3892.
[21] Popov, D., Gaponov, I., and Ryu, J. H., 2017, "Portable Exoskeleton Glove with Soft Structure for Hand Assistance in Activities of Daily Living," IEEE/ASME T. Mech., **22**(2), pp. 865–875.
[22] Koo, I., Byunghyun Kang, B., and Cho, K.-J., 2013, "Development of Hand Exoskeleton Using Pneumatic Artificial Muscle Combined With Linkage," J. Korean Soc. Precis. Eng., **30**, pp. 1217–1224.
[23] Polygerinos, P., Lyne, S., Wang, Z., Nicolini, L. F., Mosadegh, B., Whitesides, G. M., and Walsh, C. J., 2013, "Towards a Soft Pneumatic Glove for Hand Rehabilitation," Proceedings of IEEE International Conference on Intelligent Robots and Systems, Tokyo, Japan, Nov. 3–7, pp. 1512–1517.
[24] Polygerinos, P., Wang, Z., Galloway, K. C., Wood, R. J., and Walsh, C. J., 2015, "Soft Robotic Glove for Combined Assistance and At-Home Rehabilitation," Robot. Auton. Syst., **73**, pp. 135–143.
[25] Yun, S.-S., Kang, B. B., and Cho, K.-J., 2017, "Exo-Glove PM: An Easily Customizable Modularized Pneumatic Assistive Glove," IEEE Robot. Autom. Lett., **2**(3), pp. 1725–1732.
[26] Refour, E., Sebastian, B., and Ben-Tzvi, P., 2018, "Two-Digit Robotic Exoskeleton Glove Mechanism: Design and Integration," ASME J. Mech. Rob., **10**(2), p. 025002.
[27] Lin, J., Wu, Y., and Huang, T. S., 2000, "Modeling the Constraints of Human Hand Motion," Constraints, pp. 121–126.
[28] Feix, T., Romero, J., Schmiedmayer, H. B., Dollar, A. M., and Kragic, D., 2016, "The GRASP Taxonomy of Human Grasp Types," IEEE T. Hum-Mach. Syst., **46**(1), pp. 66–77.
[29] Edwards, S. J., Buckland, D. J., and McCoy-Powlen, J. D., 2002, *Developmental and Functional Hand Grasps*, 1st ed., Slack Incorporated, Thorofare, NJ.
[30] Lee, K.-S., and Jung, M.-C., 2015, "Three-Dimensional Finger Joint Angles by Hand Posture and Object Properties," Ergonomics, **12**(2), pp. 1–11.
[31] Hara, A., Amauchi, Y. Y., Kusunose, K. K., Yamauchi, Y., and Kusunose, K. K., 1994, "Analysis of Thumb and Index Finger Joints During Pinching Motion and Writing a Cross, as Measured by Electrogoniometers," *Clinical Biomechanics and Related Research*. Springer Japan, Tokyo, pp. 282–293.
[32] Lowe, B. D., Kong, Y., and Han, J., 2006, "Development and Application of a Hand Force Measurement System," Proceedings of the 16th Congress of the International Ergonomics Association, Maastricht, The Netherlands, July 10–14.
[33] Mathiowetz, V., Kashman, N., Volland, G., Weber, K., Dowe, M., and Rogers, S., 1985, "Grip and Pinch Strength: Normative Data for Adults," Arch. Phys. Med. Rehab., **66**(2), pp. 69–74.
[34] Takagi, M., Iwata, K., Takahashi, Y., Yamamoto, S. I., Koyama, H., and Komeda, T., 2009, "Development of a Grip Aid System Using Air Cylinders," Proceedings — IEEE International Conference on Robotics and Automation, Kobe, Japan, May 12–17, pp. 2312–2317.
[35] Hasegawa, Y., Mikami, Y., Watanabe, K., and Sankai, Y., 2008, "Five-Fingered Assistive Hand with Mechanical Compliance of Human Finger," Proceedings — IEEE International Conference on Robotics and Automation, Pasadena, CA, May 19–23, pp. 718–724.
[36] Arata, J., Ohmoto, K., Gassert, R., Lambercy, O., Fujimoto, H., and Wada, I., 2013, "A New Hand Exoskeleton Device for Rehabilitation Using a Three-Layered Sliding Spring Mechanism," Proceedings of IEEE International Conference on Robotics and Automation, Karlsruhe, Germany, May 6–10, pp. 3902–3907.
[37] Pratt, J., Krupp, B., and Morse, C., 2002, "Series Elastic Actuators for High Fidelity Force Control," Industrial Robot, **29**(3), pp. 234–241.
[38] Schiele, A., and Van Der Helm, F. C., 2006, "Kinematic Design to Improve Ergonomics in Human Machine Interaction," IEEE T. Neur. Syst. Rehabil. Eng., **14**(4), pp. 456–469.
[39] Jarrassé, N., and Morel, G., 2010, "A Formal Method for Avoiding Hyperstaticity When Connecting an Exoskeleton to a Human Member," Proceedings — IEEE International Conference on Robotics and Automation, Anchorage, AK, May 3–7, pp. 1188–1195.